PHOTOELECTRONS ANGULAR AND ENERGY DISTRIBUTIONS FROM LASER-IONIZED ARGON ATOM

VIOLETA M. PETROVIĆ, TATJANA B. MILADINOVIĆ

Department of Physics, Faculty of Science, Kragujevac University
Radoja Domanovića 12, 34000 Kragujevac, Serbia
E-mail: tanja.miladinovic@gmail.com

Received February 2, 2015

We theoretically reformulated non-relativistic angular and energy distribution of ejected photoelectron in the frame of the Ammosov–Delone–Krainov (ADK) theory for a linearly polarized laser field. The influence of the ponderomotive potential and the Stark shift on tunneling transition rate was considered. It is shown that these effects influence on behavior of the angular and energy spectrum as well as on the energy spectrum's width. Dependence of the angular and energy distribution from a spatial laser beam profile (Gaussian and Lorentzian) is discussed, as well as longitudinal and perpendicular width of photoelectron energy spectra.

Key words: laser beam profile, energy distribution, tunnel ionization.

PACS: 32.80-t, 32.80.Fb.

1. INTRODUCTION

The advances in ultrafast intense laser technology have triggered a key interest in strong field phenomena caused by strong field ionization processes. There are two ionization regimes: tunnel and multiphoton. The boundaries between these two regimes are floating. To determine the regime Keldysh introduced the dimensionless Keldysh parameter [1], $\gamma = \omega/\omega_t = \omega\sqrt{2E_i}\,/F$, where ω is laser frequency, m_e electron mass, E_i the unperturbed ionization energy, F the laser field strength and $\omega_t = F/\sqrt{2E_i}$ is a tunnel frequency. The atomic system of units $e = m_e = \hbar = 1$ is used throughout this paper. For $\gamma >> 1$ multiphoton ionization is dominant process while for $\gamma << 1$ tunnel. In the intermediate regime, $\gamma \approx 1$ is expected to have contributions from both ionization processes. Since then, an increasing interest for this concept has been observed [2, 3, 4, 5].

2. ANGULAR AND ENERGY DISTRIBUTION SPECTRA

Now we give a brief theoretical framework. For the case of low frequency laser field and the tunnel ionization the momentum's distribution has the form [6]:

$$W(p_{\text{II}}, p_{\perp}) = W(0)\exp\left[-\frac{p_{\text{II}}^2\omega^2(2E_i)^{3/2}}{3F^3} - \frac{(2E_i)^{1/2}p_{\perp}^2}{F}\right], \quad (1)$$

where p_{II} and $p_{\perp}$ are the longitudinal and perpendicular component of electron momentum and $W(0)$ is the tunneling rate. We used the ADK theory [6, 7], $W_{ADK} = \frac{F}{8\pi Z}\left(\frac{4eZ^3}{Fn^{*4}}\right)^{2n^*}\sqrt{\frac{3Fn^{*3}}{\pi Z^3}}\exp\left(-\frac{2Z^3}{3Fn^{*3}}\right)$ where n^* is the effective quantum number, $n^* = Z/\sqrt{2E_i}$, Z is the ion charge, $F = 27.5/(5.1\times10^9)\sqrt{I}$ and I is field intensity. For the case with nonzero initial momentum, the ionization rate is $W(0) \equiv W_{ADK} = \frac{F}{8\pi Z}\left(\frac{4eZ^3}{Fn^{*4}}\right)^{2n^*}\sqrt{\frac{3Fn^{*3}}{\pi Z^3}}\exp\left(-\frac{2Z^3}{3Fn^{*3}} - \frac{p^2\gamma^3}{3\omega}\right)$ [8]. The ionization rates in static and alternating electric field are different only by preexponential factor [9]. Because of that here it is convenient to use the parabolic coordinate to express initial momentum of the ejected photoelectrons outside of barrier, $p = \left(\sqrt{F\eta - 1} - \left(1/\eta\sqrt{F\eta - 1}\right)\right)/2$, where η is the parabolic coordinate, $\eta > 1/F$ [10]. If a system's total energy is independent of the coordinate η then momentum is conserved along the classical path *i.e.* $p_\eta = p$ [11].

The first term in exponential part of Eq. (1) describes the energy spectrum of ejected electrons along the polarization axis [12], where $p_{\text{II}} = p\cos\varphi$, and φ is the angle between the direction of the ejected electron and field polarization. For small angle follows $p_{\text{II}} = p\cos\varphi \approx p(1-\varphi^2/2!) \approx [\varphi << 1] \approx p$ and this term becomes:

$$W(p) = W(0)\exp\left[-\frac{p^2\omega^2(2E_i)^{3/2}}{3F^3}\right]. \quad (2)$$

Combining Eq. (2) with well now expressions for $E = p_{\text{II}}^2/2$ [12] this dependence may be written as the follows:

$$W(E) = W(0)\exp\left[-\frac{2E\omega^2(2E_i)^{3/2}}{3F^3}\right]. \quad (3)$$

The second term in exponential part of Eq. (1) shows the dependence of the ionization rate on the ejected electron momentum perpendicular to the polarization

axis of the filed. For small φ follows $p_{\perp} = p\sin\varphi \approx p(\varphi - \varphi^2/2!) \approx [\varphi << 1] \approx p\varphi$. With this approximation, this term we can rewrite in the form:

$$W(\varphi) = W(0)\exp\left[-\frac{(2E_i)^{1/2}p^2}{F}\varphi^2\right]. \tag{4}$$

Eq. (4) presents the angular distribution of the ionization rate of the ejected photoelectron. It is obvious that the probability is maximum at angle $\varphi = 0$ and decreases exponentially with increasing of the angle φ.

The ionization potential of an atom can change under laser irradiation. Here we analyzed the influence of two effects: the ponderomotive potential and the Stark effect. These two effect shifts up the ionization threshold of an atom. The ponderomotive potential is connected with the wiggle motion of charged particles in response to an applied laser field. For the linear laser polarization, it has the following form, $U_p = F^2/4\omega^2$ [13]. Also atom's energy levels are altered in laser field and this effect is known as the Stark effect. This displacement of the energy level is determined by expression $E_{St} = \alpha F^2/4$ [14], where α is the static polarizability of the atom [15]. Now we can express the shifted ionization potential in the form $E_{ief} = E_i + U_p + E_{St} = E_i + F^2/4\omega^2 + \alpha F^2/4$ [14].

Taking this correction into account the energy spectrum distribution, (see Eq. (3) and expression for $W(0)$ given in the text) can be writing as:

$$W_{pUpSt}(E) = W(0)\exp\left[-\frac{2E\omega^2\left(2\left(E_i + F^2/4\omega^2 + \alpha F^2/4\right)\right)^{3/2}}{3F^3}\right], \tag{5}$$

and the angular distribution (see Eq. (8)):

$$W_{pUpSt}(\varphi) = W(0)\exp\left[-\frac{\left(2\left(E_i + F^2/4\omega^2 + \alpha F^2/4\right)\right)^{1/2}p^2}{F}\varphi^2\right]. \tag{6}$$

With $W_{pUpSt}(E)$ and $W_{pUpSt}(\varphi)$ we noted that all corrections are included: initial momentum, ponderomotive and Stark shift. This notation will be used through the whole text.

From Eq. (1) follows that the width of the longitudinal photoelectron energy spectrum [16] is given by $\Delta E_{\text{II}} = 3F^3/\omega^2(2E_i)^{3/2}$ where E_i denotes initial ionization potential. When we take into account corrected ionization potential, E_{ief}, we have:

$$\Delta E_{\text{II}ef} = \frac{3F^3}{\omega^2\left(2E_{ief}\right)^{3/2}} = \frac{3F^3}{\omega^2\left(2\left(E_i + F^2/4\omega^2 + \alpha F^2/4\right)\right)^{3/2}}, \tag{7}$$

where $\Delta E_{\text{II}ef}$ is corrected width of the longitudinal photoelectron energy spectrum.

For the case of perpendicular direction to polarization axis typical value of photoelectron energy $\Delta E_{\perp} = F/(2E_i)^{1/2}$ [16] becomes:

$$\Delta E_{\perp ef} = \frac{F}{\left(2E_{ief}\right)^{1/2}} = \frac{F}{\left(2\left(E_i + F^2/4\omega^2 + \alpha F^2/4\right)\right)^{1/2}}, \tag{8}$$

where $\Delta E_{\perp ef}$ is corrected width of the perpendicular photoelectron energy spectrum.

The intensity distribution of laser beams in the focal plane of a focusing optic is important because it determines the laser-matter interaction process. We briefly analyzed the effects of the two different spatial laser beam profiles, Gaussian and Lorentzian, on the energy and the angular distributions of the ejected ionized photoelectrons spectra.

A simple laser beam usually has a Gaussian spatial intensity profile and we assumed it first [17]:

$$F_G(\rho) = F\exp\left(-2(\rho/R)^2\right), \tag{9}$$

where ρ is the axial coordinate that is normal to the light ray, $\rho = R\sqrt{1+\left(\lambda z/\pi R^2\right)^2}$ [18] and R is called the laser beam waist, which represents the smallest spot size realized at $z = 0$. By implementing this dependence into the equations for energy and angular distribution (Eqs. 5–6) we obtained:

$$W_{Gef}(E) = \frac{F_G(\rho)}{8\pi Z}\left(\frac{4eZ^3}{F_G(\rho)n_{ef}^{*4}}\right)^{2n_{ef}^*}\sqrt{\frac{3F_G(\rho)n_{ef}^{*3}}{\pi Z^3}}\times\exp\left(-\frac{2Z^3}{3F_G(\rho)n_{ef}^{*3}}-\frac{p^2\gamma^3}{3\omega}\right)$$
$$\times\exp\left(-\frac{2E\omega^2\left(2\left(E_i+F_G(\rho)^2/4\omega^2+\alpha F_G(\rho)^2/4\right)\right)^{3/2}}{3F_G(\rho)^3}\right), \tag{10}$$

and

$$W_{Gef}(\varphi) = \frac{F_G(\rho)}{8\pi Z}\left(\frac{4eZ^3}{F_G(\rho)n_{ef}^{*4}}\right)^{2n_{ef}^*}\sqrt{\frac{3F_G(\rho)n_{ef}^{*3}}{\pi Z^3}}\times\exp\left(-\frac{2Z^3}{3F_G(\rho)n_{ef}^{*3}}-\frac{p^2\gamma^3}{3\omega}\right)$$
$$\times\exp\left(-\frac{\left(2\left(E_i+F_G(\rho)^2/4\omega^2+\alpha F_G(\rho)^2/4\right)\right)^{1/2}p^2}{F_G(\rho)}\varphi^2\right), \tag{11}$$

where n_{ef}^{*} denotes the corrected effective quantum number, $n_{nf}^{*} = Z\Big/\sqrt{2E_{ief}} = Z\Big/\sqrt{2\left(E_i + F^2/4\omega^2 + \alpha F^2/4\right)}$.

Now, let us consider the case that the laser beam has the Lorentzian spatial distribution. Several spatial profiles for the Lorentz distribution can be found. We choose the following [19]:

$$F_L(\rho) = F/\left(1+(\rho/R)^2\right). \tag{12}$$

By inserting Eq. (12) into Eq. (5) and Eq. (6) for the energy distribution we obtained:

$$W_{Lef}(E) = \frac{F_L(\rho)}{8\pi Z}\left(\frac{4eZ^3}{F_L(\rho)n_{ef}^{*4}}\right)^{2n_{ef}^{*}}\sqrt{\frac{3F_L(\rho)n_{ef}^{*3}}{\pi Z^3}}\times\exp\left(-\frac{2Z^3}{3F_L(\rho)n_{ef}^{*3}}-\frac{p^2\gamma^3}{3\omega}\right)$$
$$\times\exp\left(-\frac{2E\omega^2\left(2\left(E_i+F_L(\rho)^2/4\omega^2+\alpha F_L(\rho)^2/4\right)\right)^{3/2}}{3F_L(\rho)^3}\right) \tag{13}$$

and for the angular:

$$W_{Lef}(\varphi) = \frac{F_L(\rho)}{8\pi Z}\left(\frac{4eZ^3}{F_L(\rho)n_{ef}^{*4}}\right)^{2n_{ef}^{*}}\sqrt{\frac{3F_L(\rho)n_{ef}^{*3}}{\pi Z^3}}\times\exp\left(-\frac{2Z^3}{3F_L(\rho)n_{ef}^{*3}}-\frac{p^2\gamma^3}{3\omega}\right)$$
$$\times\exp\left(-\frac{\left(2\left(E_i+F_L(\rho)^2/4\omega^2+\alpha F_L(\rho)^2/4\right)\right)^{1/2}p^2}{F_L(\rho)}\varphi^2\right). \tag{14}$$

$W_{Gef}(E)$ and $W_{Lef}(E)$ denote the energy, while $W_{Gef}(\varphi)$ and $W_{Lef}(\varphi)$ angular distribution of the ejected photoelectron for the case of the Gaussian and the Lorentzian beam profile with included fully corrected ionization potential.

3. DISCUSSION

In this paper, we observed and discussed the influence of the corrected ionization potential and the spatial profile of laser beam on the energy and angular distribution of the ejected photoelectron spectra. The calculations were made for the linearly polarized radiation with the wavelength of $\lambda = 800$ nm $(\omega = 0.05696\,\text{a.u.})$ and intensities up to $I = 10^{16}\,\text{Wcm}^{-2}$ for the argon atom, Ar.

First we analyzed the energy distribution spectra (see Eq. (3) and Eq. (5) with included in-line equation for $W(0)$ and the initial momentum, p). Corresponding

theoretical curves for the energy distribution spectra without any correction, $W(E)$ and with included nonzero initial momentum of the ejected photoelectrons $W_p(E)$ are given in Fig. 1(a).

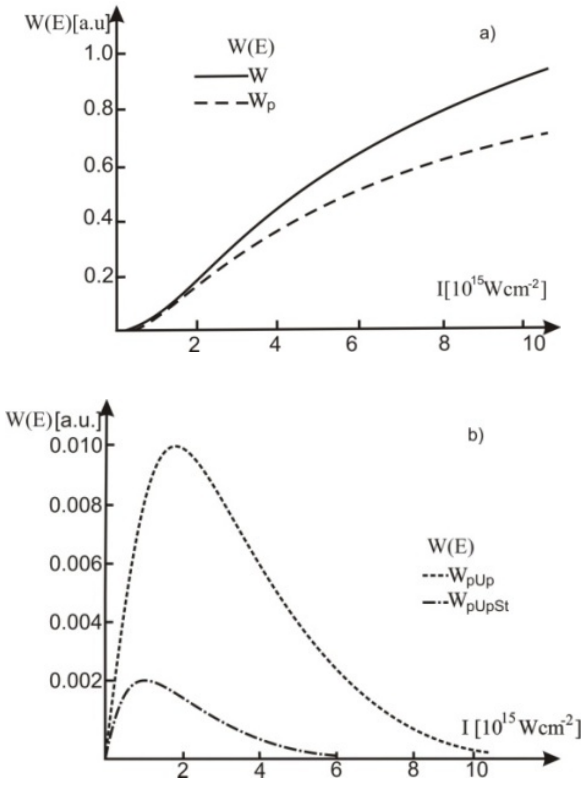

Fig. 1 – The theoretical curves for the energy distribution spectra *versus* laser field intensity. a) $W(E)$ and $W_p(E)$, b) $W_{pUp}(E)$ and $W_{pUpSt}(E)$. The value of η is fixed at 190.

This correction influences only on the value of $W(E)$, since the behavior of curve does not change. But additional corrections (ponderomotive and Stark shift) have significant influence. In Fig. 1(b) we shown obtained curves for $W_{pUp}(E)$ and $W_{pUpSt}(E)$. Both curves have the maximum, which is for the $W_{pUpSt}(E)$ shifted to the lower field intensity. Also the corresponding maximal value is reduced which is expected because the ionization energy is shifts up to higher values. The maximum of $W_{pUp\max}(E)$ appears at $I = 1.8 \times 10^{15}\ \mathrm{Wcm}^{-2}$ and for $W_{pUpSt\max}(E)$ at $I = 1.2 \times 10^{15}\ \mathrm{Wcm}^{-2}$.

The theoretical angular spectra of the ejected photoelectrons as a function of the scattering angle, φ (continuous curves in Fig. 2) are defined by Eq. (4) and Eq. (6). As a result the following graph was obtained:

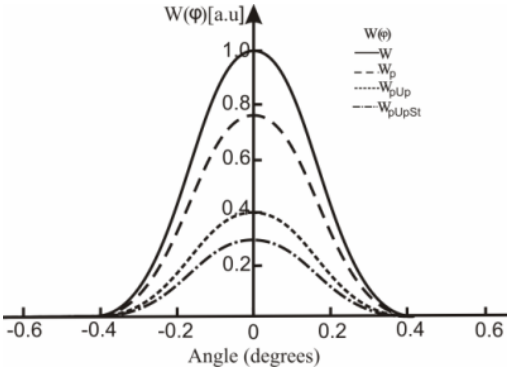

Fig. 2 – The nonrelativistic tunneling angular distribution $W(\varphi)$ *versus* the scattering angle. The laser field intensity is fixed at $I = 10^{14}\,\mathrm{Wcm}^{-2}$. The maximum occurs at $\varphi = 0$.

We calculated it step by step, so W_p has included only nonzero initial momentum of ejected photoelectrons, W_{pUp} momentum and ponderomotive potential and finally W_{pUpSt} all three mentioned effects.

Figure 2 shows that the tunneling angular distribution has the sharp maximum concentrated along the laser field direction, $\varphi = 0$ and that probability exponentially decreases with increasing of angle. The curve's shape is generally the same but incorporated effects reduce the value of the scattering probability on a given angle.

For a better understanding of these two mentioned distributions we took two different spatial laser beam profiles, Gaussian and Lorentzian. We performed this analysis for the case when all corrections are included.

In Fig. 3 we compared the spatial dependent energy distribution spectra using Eq. (10) and Eq. (13). It can be seen that the Gaussian distribution gives lower values than Lorentzian but both curves have almost the same "flow". They exponentially increase to the some maximum value and then decrease, but more slowly. For Gaussian profile the maximum is shifted to the right, *i.e.* to the higher field intensity. The laser field intensity at which is the maximal energy distribution is achieved for the Gaussian laser profile is $I = 1.3 \times 10^{15}\,\mathrm{Wcm}^{-2}$ while in the case of the Lorentzian profile at $I = 1.2 \times 10^{15}\,\mathrm{Wcm}^{-2}$.

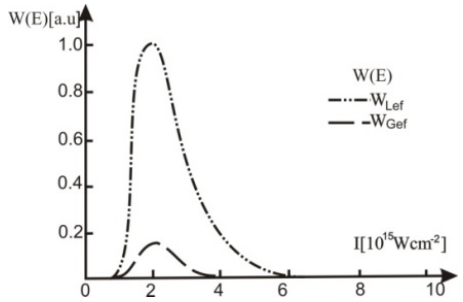

Fig. 3 – The energy distribution spectra for the Gaussian and the Lorentzian laser beam profile, $W_{Gef}(E)$ and $W_{Lef}(E)$.

Figure 4 shows calculated curves for the angular distribution spectra for Gaussian, $W_{Gef}(\varphi)$ and Lorentzian profile $W_{Lef}(\varphi)$ for two field's intensities. The graphs show that the booth curves passes through a maximum and decrease with increases of the scattering angle. For the laser field intensity $I = 10^{14}\,\mathrm{Wcm}^{-2}$ this decreasing is more quickly for the Lorentzian than for the Gaussian beam shape. In summary it is obvious that the laser field intensity plays an important role here which Fig. 4 illustrates very well.

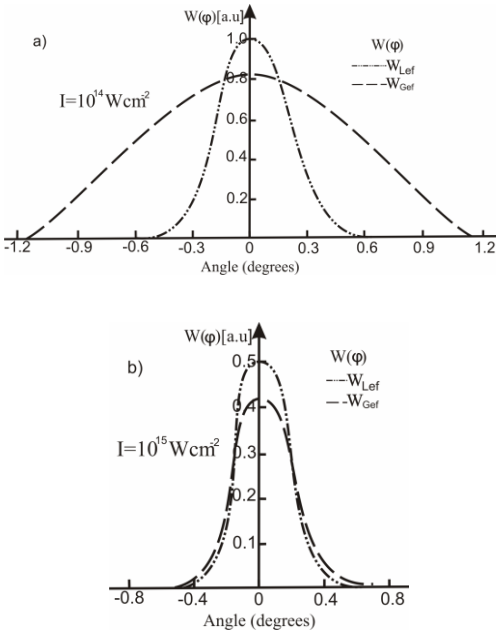

Fig. 4 – The angular distribution of the ejected photoelectrons $W_{Lef}(\varphi)$ and $W_{Gef}(\varphi)$ as the function of the scattering angle φ. a) $I = 10^{14}\,\mathrm{Wcm}^{-2}$, b) $I = 10^{15}\,\mathrm{Wcm}^{-2}$.

Next, we draw the width of the longitudinal and perpendicular energy spectrum. As a result, based on Eq. (7) the following graphs are obtained:

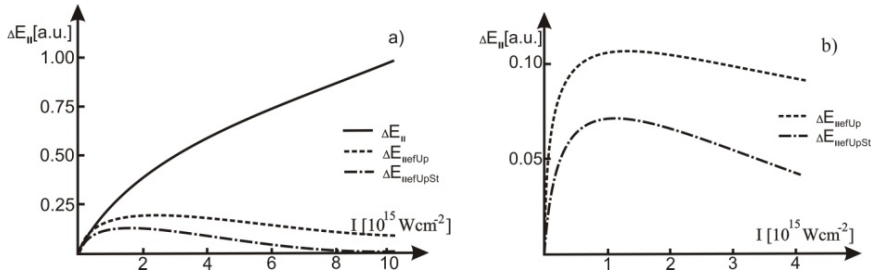

Fig. 5 – The corrected width of the longitudinal photoelectron energy spectrum a) ΔE_{II} , $\Delta E_{\text{II}efUp}$ and $\Delta E_{\text{II}efUpSt}$ b) Zoomed part of graph 6a), $\Delta E_{\text{II}efUp}$ and $\Delta E_{\text{II}efUpSt}$.

From Fig. 5 (a) we see that inclusion of the shifted potential has significant influence on the behavior of the width of the longitudinal photoelectron spectrum. Now we have maximum of the energy's width at some particular value of the field intensity and which is shifted to the lower laser field intensities Fig. 5 (b) when the Stark shift is taken into account.

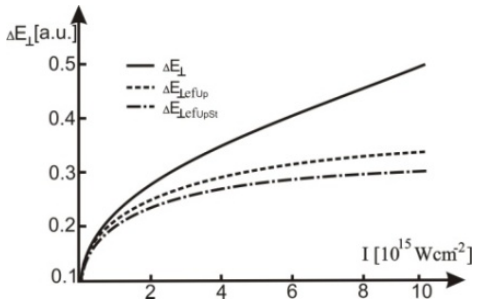

Fig. 6 – The corrected width of the perpendicular photoelectron energy.

Figure 6 shows the predictions of Eq. (8). The same notation as in Fig. 5 is used. It is obvious that the influence of the ponderomotive and the Stark sift is less for the case of perpendicular energy width.

We also compared the spatial dependence for the width of the longitudinal and perpendicular energy spectrum respectively. For this purpose first, we inserted Eq. (9) in Eq. (7) and obtained longitudinal width for the Gaussian laser beam with included all corrections of the ionization potential in the following form:

$$\Delta E_{\text{II}Gef} = \frac{3F_G(\rho)}{\omega^2\left(2\left(E_i + F_G(\rho)^2/4\omega^2 + \alpha F_G(\rho)^2/4\right)\right)^{3/2}} . \tag{15}$$

Using Eq. (7) and Eq. (12), analogously to previous procedure, we obtained width for the Lorentzian laser beam, $\Delta E_{\text{II}Lef}$.

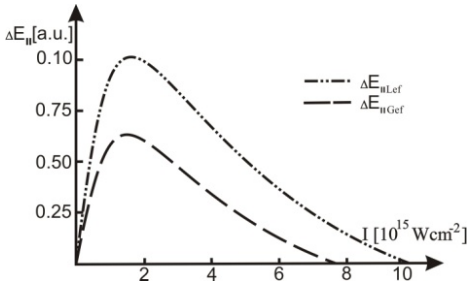

Fig. 7 – The longitudinal width for the Gaussian, $\Delta E_{\text{II}Gef}$ and the Lorentzian, $\Delta E_{\text{II}Lef}$ laser beam.

Figure 7 shows calculated curves of $\Delta E_{\text{II}ef}$ for two different spatial pulse shapes. It can be seen that the spatial profile influences on the behavior of the longitudinal width. Lorentzian gives the higher maximal value and also shifts corresponding laser field intensity to higher value.

Finally, we analyzed the perpendicular width of energy spectrum. Combining Eq. (8) and Eq. (9) we obtained the Gaussian perpendicular width:

$$\Delta E_{\perp Gef} = \frac{F_G(\rho)}{\left(2\left(E_i + F_G(\rho)^2/4\omega^2 + \alpha F_G(\rho)^2/4\right)\right)^{1/2}}, \tag{16}$$

and on the same way, combining Eq. (8) and Eq. (12), the Lorentzian perpendicular width with included all corrections of the ionization potential.

Graph 8 shows both obtained perpendicular widths.

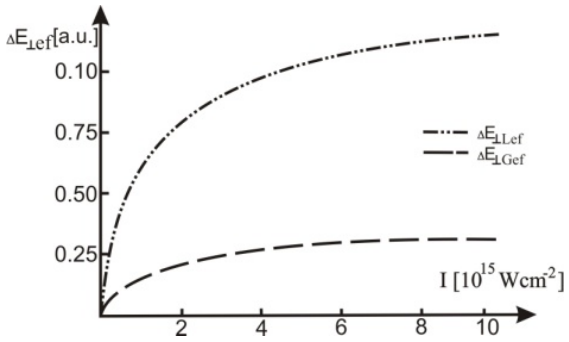

Fig. 8 – The perpendicular width for the Gaussian, $\Delta E_{\perp Gef}$ and the Lorentzian, $\Delta E_{\perp Lef}$ laser beam.

It is clear that the spatial profile influences only on the value of considered perpendicular width.

4. CONCLUSION

In this paper, we reported our calculations of the energy and the angular distribution spectra of photoelectrons emitted by atoms in intense laser field for the regime of tunnel ionization. The influence of the shifted ionization potential caused by the ponderomotive and Stark shift is considered, as well as the nonzero initial momentum of the ejected photoelectron. Also we applied two different spatial profiles on analyzed distribution. Our results we presented graphically. We found that all mentioned effects contribute to the behavior of both distributions and must be taken into account. Also we showed that spatial profile of a laser beam more or less plays a role in the behavior of considered variables.

Acknowledgements. We are grateful to the Serbian Ministry of Education and Science for financial support through Projects 171020 and 171021.

REFERENCES

1. L.V. Keldysh, *Ionization in the Field of a Strong Electromagnetic Wave*, Soviet Physics JETP **20**, 1307–1314 (1965).
2. S. B. Popruzhenko, V. D. Mur, V. S. Popov, and D. Bauer, *Multiphoton Ionization of Atoms and Ions by High Intensity X Ray Lasers*, Journal of Experimental and Theoretical Physics, 2009, Vol. **108**, No. 6, pp. 947–962 (2009).
3. R. Murray, *Tunnel Ionization in Strong Fields in atoms and molecules and its applications*, Phd. thesis, University of Waterloo, Ontario, Canada (2011).
4. M.M. Radulović, J.M. Stevanović, T.B. Miladinović and V.M. Ristić, *The role of the non-zero initial momentum and modified ionization potential in the corrected Ammosov-Delone-Krainov theory*, Romanian Journal of Physics, Vol. **58**, Nos. 1–2, 127–135 (2013).
5. X. M. Tong, P. Ranitovic, D. D. Hickstein, M. M. Murnane, H. C. Kapteyn, and N. Toshima, *Enhanced multiple-scattering and intra-half-cycle interferences in the photoelectron angular distributions of atoms ionized in midinfrared laser fields*, Physical Review A **88**, 013410-5 (2013)
6. N.B. Delone and V.P. Krainov, *Multiphoton Processes in Atoms*, 2nd edition (New York: Springer, 2000).
7. V.M. Ammosov, N.B. Delone, and V.P Krainov, *Tunnel ionization of complex atoms and of atomic ions in an alternating electromagnetic field*, Soviet Physics JETP **64**, 1191–1194 (1986).
8. V.M. Ristić, T.B. Miladinović and M.M. Radulović, *Analyzing the Transition Rates of the Ionization of Atoms by Strong Fields of a CO2 Laser Including Nonzero Initial Momenta*, Laser Physics **18**, 1183-1187 (2008).
9. A.M. Perelomov, V.S. Popov and M.V. Terentev, *Ionization of atoms in an alternating electric field*, Soviet Physics JETP **23**, 924–934 (1966).
10. D. Bauer, *Theory of Intense Laser-Matter Interaction*, Max-Planck-Institut für Kernphysik, Heidelberg (2006), p. 57–58.
11. L.D. Landau and E.M. Lifshitz, *Quantum Mechanics: Non-Relativistic Theory*, 3rd edition, (Oxford: Pergamon, 1991), §77, pp. 298.
12. N.B. Delone, I. Yu. Kiyan and V. P. Krainov, *Ionization of atoms by a strong low-frequency field*, Laser Physics, Vol. **3**, No. 2, 312-322 (1993), www.maik.ru/full/lasphys_archive/93/2/lasphys2_93p312full.pdf.
13. T.B. Miladinović and V.M. Petrović, *Quasiclassical approach to tunnel ionization in the non relativistic and relativistic regimes*, Revista Mexicana de Física, **60**, 290–295 (2014).

14. E. A. Volkova, A. M. Popov, and O. V. Tikhonova, *Ionization and stabilization of atoms in a high-intensity low-frequency laser field*, Journal of Experimental and Theoretical Physics, Vol. **113**, No. 3, 394–406 (2011).
15. http://ctcp.massey.ac.nz/Tablepol2014.pdf.
16. N.B. Delone and V.P Krainov, *Tunneling and barrier-suppression ionization of atoms and ions in a laser radiation field*, Physics - Uspekhi Vol. **41**, No. 5, 469–485 (1998).
17. V.N. Tokarev, J. Lopez, S. Lazare, and F. Weisbuch, *High-aspect-ratio microdrilling of polymers with UV laser ablation: experiment with analytical model*, Applied Physics A **76**, 385–396 (2003).
18. L. Zhang, *Intensity spatial profile analysis of a Gaussian laser beam at its waist using an optical fiber system*, Chinese Physics Letters, **27**, No. 5, 054207-3 (2010).
19. S.L. David and H.A. John, *Beam shaping profiles and propagation, Proceedings SPIE Conf. Laser Beam Shaping VI*, (San Diego, California, USA, 2005), pp. 5876–13, http://people.cas.uab.edu/~dls/publications/spie5876/spie5876-13-electronic.pdf.